ADVANCED FUNCTIONAL MATERIALS
www.afm-journal.de

Upgraded Structure and Application of Coal-Based Graphitic Carbons Through Flash Joule Heating

Sheng Zhu, Chong Guan, Yating Wu, Jiangfeng Ni,* and Gaoyi Han**

Facilitating the transition and new application of fossil energy sources are crucial to attaining carbon neutrality. Conversion of coals into graphitic carbons represents an effective route to achieve their high-value utilization, while this process always involves corrosive/toxic chemical reagents and time-intensive heating treatment. Here, this work reports a green, rapid, and efficient flash Joule heating (FJH) technique to produce high-quality carbons from diverse coals within 1 s. The surface groups, defects, and graphitization degree of the resultant carbon materials are controlled during the instantaneous thermal shock process, and the relationships between the coal structures and the product properties are established. The results suggest that the anthracite with high coalification degree tends to form highly graphitic carbons at a peak temperature of ≈3300 K, presenting higher rate capability (79.1% capacity retention at 30 A g^{-1}) and low relaxation time constant (τ_0 = 0.27 s) toward capacitive energy storage. Besides, the flash carbon materials derived from lignite and bituminous coal with low coal rank show better capacitive performance with capacity above 80 F g^{-1} at 1 A g^{-1}. This study evidences that the FJH technology holds great potential to steer coals into valuable carbon materials.

1. Introduction

Coal stands as a kind of significant fossil energy source, contributing to about 27% of the global primary energy consumption. After million years of geographical evolution, there emerge different types of coal mines with distinguishable differences in their composition and structure.[1,2] For example, anthracite features highest carbon content (>90%) and low volatile dry-free basis (V_{daf}, <10%),[3,4] whereas lignite possesses a low ignition point of 300–400 °C and approximately 40% volatile matters.[5] Bituminous coal falls in between, boasting a carbon content range of 75%–90%.[6,7] Due to the economical advantage and high carbon content, converting coal into carbon nanomaterial has garnered considerable attention, particularly in energy storage, catalysis, adsorption, and electronics related fields.[8–10] Although the coal structure is complex, understanding the structure evolution during the conversion process is crucial for controlling the structure and property of the resultant carbon materials.

In recent years, coal-derived carbon materials have been widely reported encompassing graphite,[11] graphene,[12,13] carbon nanotubes,[14] and porous carbon.[15–17] Generally, their preparations demand thermal annealing and/or chemical activation processes. Chemical activation involves creation of nanopores by destroying carbon structure with strong acids or alkalis.[18,19] Thermal annealing can repair structure defects by dehydrogenation and deoxidation under high-temperature to produce high-purity coal-based carbon materials.[20,21] However, currently widely used heating technique such as conventional furnaces are considerably time- and/or energy-consuming, arc discharge, and laser etching hinder large-scale production due to the harsh preparation conditions and expensive devices.[22,23] Therefore, it is very necessary to develop convenient and cost-effective methods for producing coal-based carbon materials. Recently, the flash Joule heating (FJH) technique has been widely reported to prepare pitch or anthracite-derived graphene materials, their applications in supercapacitors, corrosion resistance, and lubricating oils are explored.[24–29] As an emerging synthetic method, FJH exhibits great superiorities of environmental-friendliness, high efficiency, low time, and energy consumption, making it promising in transforming various coals into high-value carbon materials.

S. Zhu, C. Guan, Y. Wu, G. Han
Institute of Molecular Science
Key Laboratory of Chemical Biology and Molecular Engineering of Education Ministry
Shanxi University
Taiyuan 030007, China
E-mail: shengzhu@sxu.edu.cn; han_gaoyis@sxu.edu.cn

S. Zhu
Institute for Carbon-Based Thin Film Electronics
Peking University
Shanxi (ICTFE-PKU), Taiyuan 030012, China

S. Zhu
Jiangsu Key Laboratory of Frontier Material Physics and Devices
Soochow University
Suzhou 215006, China

J. Ni
School of Physical Science and Technology
Center for Energy Conversion Materials & Physics (CECMP)
Jiangsu Key Laboratory of Frontier Material Physics and Devices
Jiangsu Key Laboratory of Advanced Negative Carbon Technologies
Soochow University
Suzhou 215006, China
E-mail: jeffni@suda.edu.cn

The ORCID identification number(s) for the author(s) of this article can be found under https://doi.org/10.1002/adfm.202403961

DOI: 10.1002/adfm.202403961

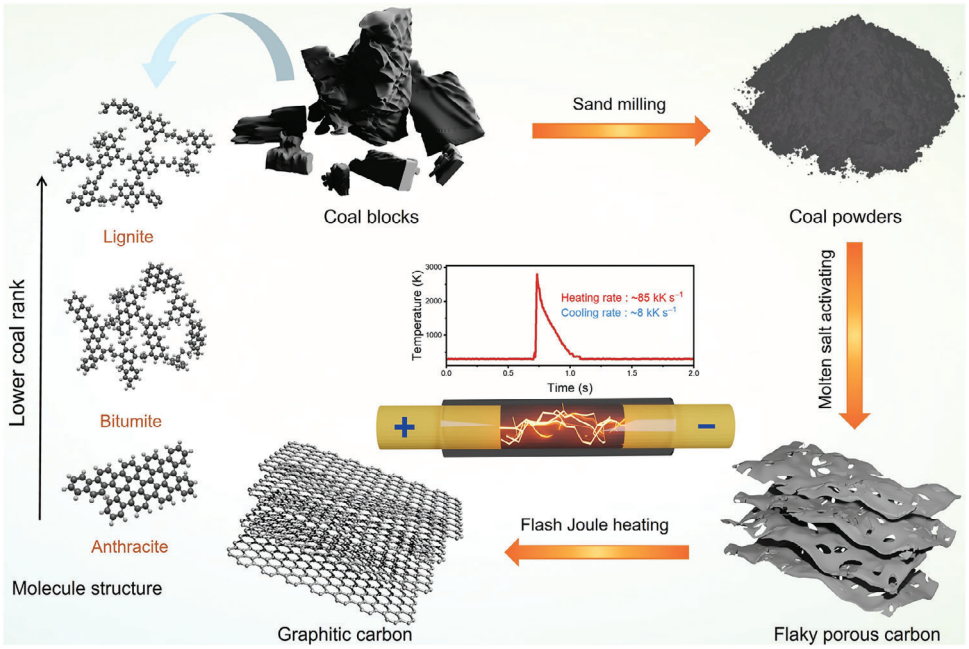

Figure 1. Schematic illustration for preparation of coal-based graphitic carbon materials through flash Joule heating (FJH).

In this work, we report a general and universal method to prepare graphitic carbons from different types of coals by FJH technique combined with the molten-salt pretreatment. The FJH process is simple and effective, which is free of chemical reagents, catalysts, and special gases. During the flash process, the rapid deoxidation couples with the continuous condensation of aromatic rings, leads to the formation of carbon materials from amorphous to graphitized structure. The parameters in FJH treatment are optimized to modulate the composition and structure evolutions of resultant carbon materials including surface groups, porosities, defects, and graphitization degree. Besides, the relationship between coal feedstocks and prepared carbon products is studied by the electron microscopies, spectroscopic techniques, electrochemical analyses, and molecular dynamics simulations. The coal with high coalification degree tends to form highly graphitic carbons, featuring high rate capability and low relaxation time constant toward capacitive energy storage.

2. Results and Discussion

The preparation pathway of coal-based graphitic carbon materials is elucidated in **Figure 1**. We utilize three types of coals including lignite, bituminous coal, and anthracite as feedstocks, their molecule structure models are sequentially supplied based on the coalification ranks. Typically, the coal feedstocks suffer from poor conductivities due to the existence of impurities, which demand pretreatment or incorporation with conductive agents during FJH execution. Here, molten-salt activation in KCl/K_2CO_3 media is conducted after sand milling, eliminating impurities and enhancing conductivity of coals, as well as facilitating the exfoliation into two-dimensional (2D) nanoflakes. During the FJH process, the capacitor undergoes rapid discharge and applies voltage on both sides of the sample to induce instantaneous thermal shock. The equipment setup for FJH is shown in Figure S1 (Supporting Information), which encompasses the display system, reaction system, and control system for adjusting the flash parameters. As illustrated in the time-temperature diagram, upon the release of the applied voltage, wherein almost all the electric energy is converted into heat energy. The temperature rapidly ascends to near 3000 K at an impressive rate of 85 kK s^{-1}, and then followed by a swift cooling to room temperature at 8 kK s^{-1}. The entire FJH synthesis process is accomplished in less than 1 s, such expeditious thermal processing effectuates the production of graphene-like materials.

Generally, the aromatic hydrocarbon skeleton, aliphatic chain, and C=O content constitute the primary factors reflecting the structure and quality of coal-derived products.[2,30] **Figure 2**a–c presents 2D molecular structure models corresponding to lignite, bitumite, and anthracite, respectively. With the progression of the coalification degree, the oxygen content gradually decreased, accompanied by the emergence of aromatic fragments with larger sizes.[31,32] Figure S2 (Supporting Information) shows the thermogravimetry-derivative thermogravimetry (TG-DTG) curves of the raw bitumite and the sample after direct flash treatment, and both show high content of residues including inorganic impurities and ashes after heating treatment. The X-ray diffraction (XRD) pattern of raw bitumite-F also confirms the presence of inorganic impurities (Figure S3, Supporting Information). Therefore, molten-salt activation in KCl/K_2CO_3 media was conducted before FJH process to address this issue (Figure S4, Supporting Information). Furthermore, the thermogravimetry-mass spectrometry-infrared (TG-MS-IR) coupling technique was utilized to investigate the function of KCl/K_2CO_3 molten salts in structure modulation during the pyrolysis process. The TG curves of KCl/K_2CO_3+bitumite composite in Figure S5a (Supporting Information) reveal two primary temperature regions of mass loss, with one at 84.1 °C corresponding to the evaporation of water. Another significant mass change

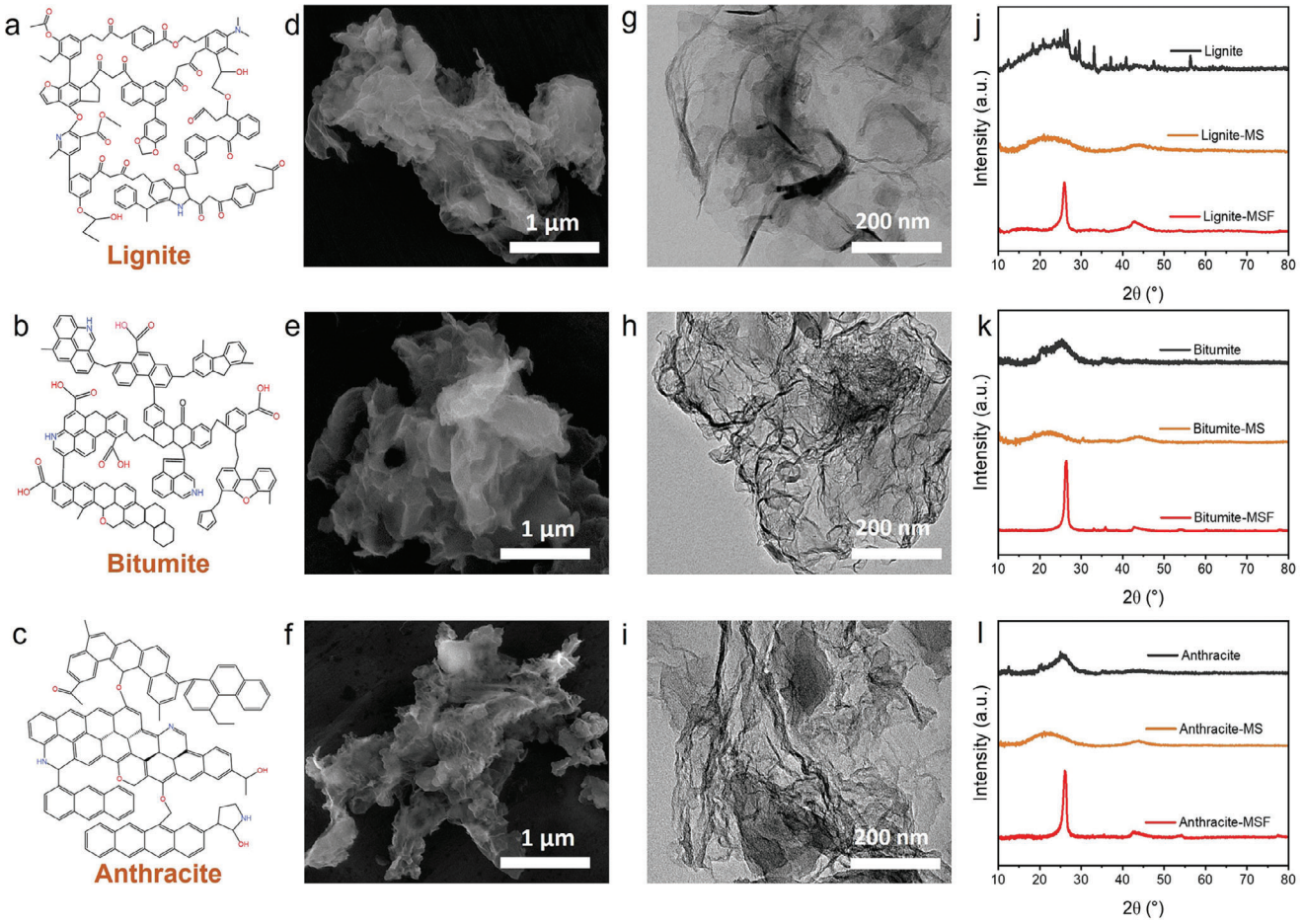

Figure 2. a–c) Molecular structure models of lignite, bituminous coal, and lignite. d–f) Scanning electron microscopy (SEM) images of lignite-MSF, bitumite-MSF, and anthracite-MSF. g–i) Transition electron microscopy (TEM) images of lignite-MSF, bitumite-MSF, and anthracite-MSF. j) X-ray diffraction (XRD) patterns of lignite, lignite-MS, and lignite-MSF. k) XRD patterns of bitumite, bitumite-MS, and bitumite-MSF. l) XRD patterns of anthracite, anthracite-MS, and anthracite-MSF.

at 667 °C is attributable to the molten salts transitioning from solid to liquid state, fully encapsulating the bitumite for activation. As shown in Figure S5b–c (Supporting Information), the absorption peaks at 3500 and 1508 cm^{-1} correspond to the evaporation of moisture and the generation of a substantial amount of CH_4 due to the breaking of aliphatic chains.[33] K_2CO_3 acts as the main activator to form rich porous structure during the pyrolysis process by producing CO_2 (2361 cm^{-1}) and a small amount of CO. Based on the above analyses, the possible reaction equations are summarized as follows:

$$K_2CO_3 \rightarrow K_2O + CO_2 \uparrow \quad (1)$$

$$K_2CO_3 + 2C \rightarrow 2K + 3CO \uparrow \quad (2)$$

$$K_2O + C \rightarrow 2K + CO \uparrow \quad (3)$$

After being pretreated in the molten-salt medium, lignite-MS, bitumite-MS, and anthracite-MS are obtained from the corresponding coals. Scanning electron microscopy (SEM) images (Figure S6, Supporting Information) depict the formation of flaky porous carbon for all three coals after molten-salt etching, particularly for lignite and bitumite, owing to their lower coalification degree and weaker structural rigidity. Subsequently, the porous carbons undergo the flash treating at 140 V to generate the corresponding products of lignite-MSF, bitumite-MSF, and anthracite-MSF. The SEM (Figure 2d–f) and transition electron microscopy (TEM) images (Figure 2g–i) display their evident layered morphology compared to the blocky appearance of the initial coals (Figure S7, Supporting Information). The high-resolution TEM images show distinctive lattice fringes (Figure S8, Supporting Information), validating the formation of carbon materials with high graphitization degree after instantaneous thermal shock. This is also confirmed by the XRD patterns with the sharp peak near 26°, corresponding to the diffraction of C(002) plane.[34,35] The interlayer spacing $d_{(002)}$ can be determined by the formula: $d_{(002)} = \lambda/2\sin\theta_{(002)}$ (where λ is the wavelength of the ray (0.15 405 nm) and $\theta_{(002)}$ is the angle corresponding to the (002) peak). The $d_{(002)}$ values of lignite-MSF, bitumite-MSF, and anthracite-MSF are 0.343, 0.338, and 0.341 nm, respectively.[36,37] Furthermore, these XRD patterns (Figure 2j–l) only show the characteristic signal of carbon, indicating the effective removal

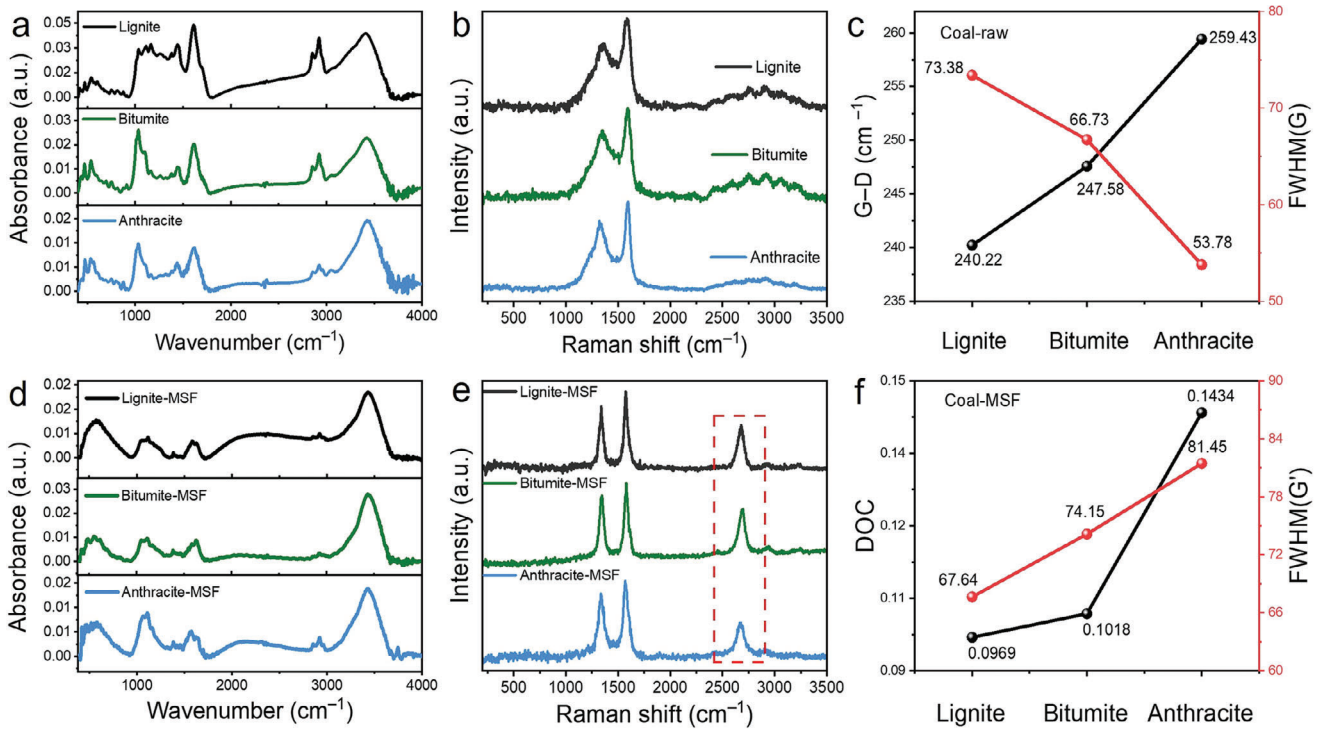

Figure 3. a) Infrared spectra and b) Raman spectra of different coals. c) G–D and full width at half maximum (FWHM) (*G*) analyses of different coals. d) Infrared spectra and e) Raman spectra of lignite-MSF, bitumite-MSF, and anthracite-MSF. f) DOC and FWHM (*G'*) analyses based on Raman spectra and infrared spectra.

of impurities in coal after molten salts and FJH treatments. Bitumite-MSF exhibits higher pyrolysis temperature (Figure S9, Supporting Information), indicating the ultrafast Joule heating allows for the formation of carbon materials from amorphous to graphitic structure. The element analysis (EA) results of different samples are compared in Figure S10 (Supporting Information). Furthermore, pitch was also studied as a precursor, and SEM images in Figure S11 (Supporting Information) show a honeycomb morphology for both pitch-MS and pitch-MSF. The exfoliating effect is notably superior to that of coal-based products, attributing to the softer texture and higher malleability of pitch.[22]

In-depth understanding of the molecular structure and chemical composition of coal feedstocks is imperative for their upgrading in terms of structure and application. Infrared spectrum proves to be an effective tool for discerning the internal molecular structure of various coal types.[38,39] The Fourier transform infrared (FTIR) spectra of three coals are presented in **Figure 3**a, and the corresponding fitting curves are elucidated in Figure S12 (Supporting Information), wherein the specific functional groups are identified, facilitating an insightful analysis of the coal structure. The bands at 2800–3000 cm^{-1} encompasses aliphatic hydrocarbon functional groups such as $-CH_2-$ and $-CH_3$,[36] while the bands at 1650–1800 cm^{-1} and 1590–1610 cm^{-1} correspond to C=O and C=C functional groups, respectively. The peak at the 700–900 cm^{-1} arises from aromatic C—H out-of-plane bending modes.[38] Table S1 (Supporting Information) provides the data obtained by calculating integral areas of specific peaks in the infrared spectra of three types of coals, parameter I reflects the coal aromaticity, parameter 'C' is derived from the integral peak area corresponding to the C=O bond, indicating coal maturity, and DOC represents the ratio of integral peak areas in the range of 700–900 cm^{-1} and around 1600 cm^{-1}, signifying the condensation degree of aromatic rings.[38] As coal rank increases, the parameters I and DOC gradually increase, suggesting a continuous condensation of aromatic rings during the coalification process (Figure S13, Supporting Information). Conversely, the decrease of 'C' indicates that the higher rank coal corresponds to less C=O groups, indicative of a relatively lower oxygen content. Notably, anthracite exhibits the lowest oxygen content and aliphatic chain, while lignite boasts the highest.

For Raman spectra of carbon materials, the D band situated at ≈1350 cm^{-1} is originated from the C—C bonds between aromatic rings and aromatic compounds with no fewer than six rings, while the G peak at 1580 cm^{-1} corresponds to the aromatic ring quadrant breathing or C=C bonds of alkenes.[40,41] As shown in Figure 3b–c, the G–D (position difference between the G and D bands) and full width at half maximum (FWHM) of the G band serve as indicators for analyzing the coalification degree of different coals. A larger value of G–D, along with a narrower FWHM (G), suggests a higher degree of graphitization and increased maturity.[42] After molten-salt pretreatment, coal raw materials form porous amorphous carbon without detectable impurities. Figure S14 (Supporting Information) depicts the Raman spectra of lignite-MS, bitumite-MS and anthracite-MS, showcasing different structures of these porous carbons. The I_D/I_G ratio becomes instrumental in measuring the defects of carbon materials. Lignite-MS and bitumite-MS display massive defect structures maybe due to many volatile organic compounds (VOCs)

in lower-grade coals, the decomposition of organic components would generate pore structure during molten-salt activation.[15] Conversely, anthracite-MS exhibits the smallest I_D/I_G ratio owing to its fewer VOCs and higher coalification degree.

Upon flashing at 140 V, the reduction in peak intensity between 1650 and 1800 cm^{-1} (C═O) also reveals a decrease of oxygen content in these carbon materials (Figure 3d). Furthermore, sharper and more symmetrical G peak indicates the transformation of C—C bonds into C═C bonds (Figure 3e), a smaller I_D/I_G ratio also signifies the defect repairation during the FJH process.[43] Besides, the G′ peak near 2750 cm^{-1} indicates graphite stacking, an obviously sharp and symmetric peak in the carbon materials after flashing signifies enlarged interlayer spacing.[44,45] The distinct structures of the three types of coals yield different products after flashing. The DOC values of lignite-MSF, bitumite-MSF, and anthracite-MSF are 67.64, 74.15, and 81.45 respectively (Figure 3f), which mean that anthracite-MSF possesses the higher degree of aromatic ring condensation and large size aromatic fragment. However, the intensities of G' peaks of lignite-MSF and bitumite-MSF surpass that of anthracite-MSF, and the FWHM (G') after Joule heating correlates positively with the coalification degree of the initial coal, considering the understanding of the structures of different coals. It can be inferred that the substantial number of aliphatic chains in lignite and bituminous coal provide a larger H:C ratio and rich C═O bonds, supplying more free radicals for recombination during the flash process.[24,46] Therefore, carbon materials synthesized from low-rank coal exhibit a more pronounced stacking effect. In contrast, anthracite yields a lower graphite stack due to its higher degree of coalification and stronger structural rigidity caused by long range ordered molecular structure arrangement. The same trend is observed when using pitch as the precursor (Figure S15, Supporting Information), and the I_D/I_G ratio of pitch-MSF is mere 0.063, displaying sharper G peak and G' peak in Raman spectra (Figure S16, Supporting Information). These results underscore the superior quality of carbon material synthesized from pitch, attributed to the easier rearrangement of aromatic fragments during the FJH process.

To further explore the mechanism governing the transformation from amorphous carbon to graphitization in the FJH process, our research focuses on bituminous coal with a moderate alkane concentration and medium aromatic nucleus size. We studied the impact of different flashing voltages on the structure of the carbon materials. **Figure 4a** illustrates the temperature-dependent voltage diagram, revealing a direct proportionality between applied voltage and temperature. Notably, the temperature can surpass 3800 K at 160 V. With the increase of applied flashing voltage, the intensity of the C(002) peak for the carbon material significantly rises (Figure 4b), indicating a positive correlation between the applied voltage and the crystallinity of the prepared materials. Figure 4c displays the infrared spectra of the sample after flashing at different voltages, and the corresponding data in Table S3 (Supporting Information) are calculated from it. A noticeable reduction in $A_{1650–1800}$ suggests a significant decrease in oxygen content after Joule heating. The DOC values for samples of 100, 120, 140, and 160 V are 0.02, 0.04, 0.1, and 0.14, respectively (Figure 4d), affirming that higher voltage expedites the condensation reaction of aromatic rings.

Figure S17a–e (Supporting Information) shows the N_2 adsorption–desorption isotherms and pore size distributions of bitumite-MS and samples prepared at different flash voltages. As the FJH voltage increases, the pore size distributions of different products are similar, whereas the BET surface areas and porosities decrease (Figure S17f, Supporting Information). After FJH treatment, the yields are 92.5%, 90.0%, 83.8%, and 75.0% at 100, 120, 140, and 160 V, respectively (Figure S18a, Supporting Information). As depicted in Figure 4e, the X-ray photoelectron spectra (XPS) full spectra mainly show C 1s and O 1s signals, indicating the absence of other impurity elements. As the FJH voltages increase, the oxygen ratio decreases from 9.33 at% in bitumite-MS to 3.34 at% at 160 V. Additionally, the fitting analyses of C 1s peak (Figure 4f) show a gradual decrease in matching C—O/C—C and C═O at 285.5 and 288.5 eV, while the ratio of C—C/C═C increases with rising applied voltages.[47,48] The selectivity of graphite is determined by the ratio of sp^2 carbon, as depicted in Figure S18b (Supporting Information), the sp^2 ratio increases with elevating the FJH voltages, implying the increased graphitization proportion. Further, the above experimental results are confirmed by the molecular dynamics simulations (Figure S19, Supporting Information). Initially, a prototype flaky carbon material model containing pores and irregular morphology is developed to represent the precursor obtained after the molten-salt pretreatment. During FJH process, the simulation results indicate that the carbon nanosheets gradually became uniform due to the elimination of unstable aliphatic chains and polycyclic rings after treatment at 2000 K. As the temperature escalates, the porosity within the nanosheets is notably reduced, culminating in the complete disappearance of the structure defects. The Raman spectra are shown in Figure 4g. With increasing the voltage from 100 to 160 V, the D band gradually weakens whereas the G' band begins to appear and gradually sharpen. I_D/I_G, FWHM (G), and FWHM (G') aid in understanding the effects of flash voltages on the structure of synthetic materials (Figure 4h). The I_D/I_G value decreases from 1.201 of bitumite-MS to 0.195 of bitumite-MSF at 160 V, indicating that the high temperature shock has a better repairing effect on the structure defects caused by molten-salt pretreatment. The narrower FWHM (G) suggests a significant improvement in the graphitization degree of carbon materials.[49] Similar trends are observed when lignite, anthracite, and pitch as precursors (Figures S20 and S21, Supporting Information). These analyses collectively demonstrate that the unique instantaneous heating and cooling in FJH can effectively arrange aromatic fragments, promoting the formation of materials with high graphitization degree. The above results prove that carbon materials with different structures can be modulated by changing flash parameters and coal types.

The ability in tuning defect concentration, oxygen content, and graphitization degree enables FJH technique to prepare property-controllable coal-based carbon materials. Electrochemical properties of the prepared materials, including porous carbon materials pretreated by molten-salt medium and graphitic carbon materials after FJH, have been evaluated. Firstly, the differences between the three kinds of coals after molten-salt pretreatment are investigated. As depicted in Figure S22 (Supporting Information), the presenting cyclic voltammetry (CV) profiles of lignite-MS, bitumite-MS, and anthracite-MS exhibit rectangular-like shapes, indicating typical electric double-layer capacitor (EDLC)

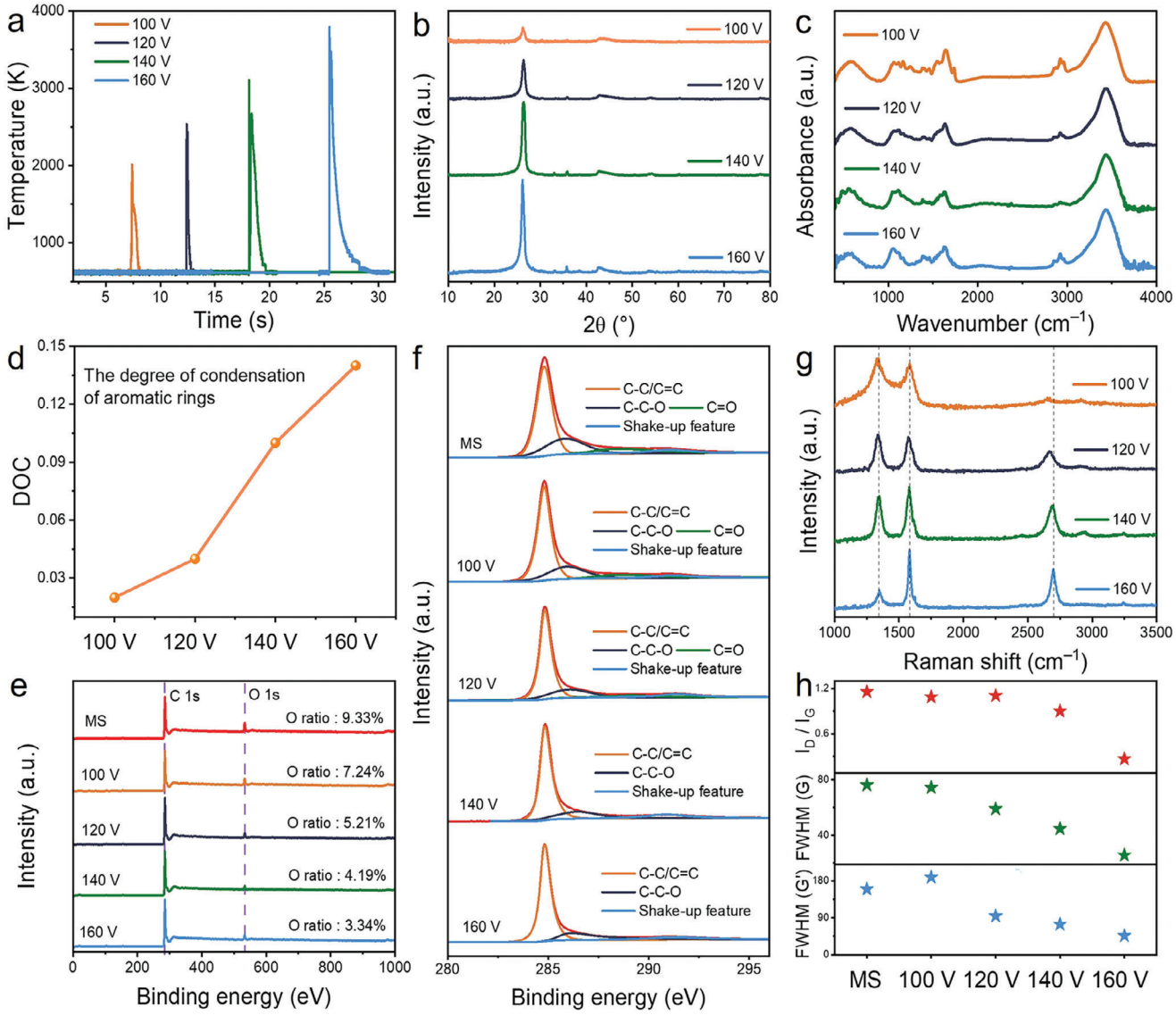

Figure 4. a) Temperature-dependent voltage diagram. b) X-ray diffraction (XRD) patterns and c) infrared spectra of samples prepared at different applied flashing voltages. d) DOC curve of samples prepared at different applied flashing voltages, e) X-ray photoelectron spectra (XPS) spectra of the precursor and samples prepared at different applied flashing voltages. f) High resolution C 1s spectra of bitumite-MS and samples prepared at different voltages. g) Raman spectra of samples prepared at different applied flashing voltages. h) I_D/I_G, FWHM (*G*) and FWHM (*G'*) analysis diagram based on Raman spectra.

behavior.[50,51] Figure S23 (Supporting Information) illustrates the specific capacitances of the coal-derived carbons after molten-salt activation under different current densities. The improved capacitance performance with decreased coalification degree can be explained by the higher presence of VOCs in lower rank coal. The coal texture may exert crucial influence on the molten-salt etching effects, for example, higher coalification degree is not conducive to exfoliation of anthracite. Additionally, pitch-MS exhibits a very high specific capacitance (306 F g^{-1} at 1 A g^{-1}) due to its relatively soft texture (Figure S24, Supporting Information).

As shown in **Figure** 5a, the specific capacitances of lignite-MS, 100, 120, and 140 V are 254.5, 136, 123.1, and 95.4 F g^{-1} at 1 A g^{-1}, respectively. The higher flash voltage leads to the reduced capacity values, which is due to the decreased defect sites and oxygen-containing groups at high temperature. Similar trends have been observed in other two types of coal-based carbon materials (Figure 5b–c). It is obvious that electrochemical performance of the flash products is highly related to the coalification degree of initial coal feedstock. The graphitic carbon materials derived from lignite and bituminous coal with low coal rank show higher capacitances at different flash voltages (Figure 5d), while anthracite-MSF features superior rate capability with a capacity retention of 79.1% at 30 A g^{-1} (Figure S25, Supporting Information). Besides, the Bode plots of lignite-MSF, bitumite-MSF, and anthracite-MSF are shown in Figure 5e. The corresponding frequency (f_0) of anthracite-MSF at the phase angle of –45° is higher than that of lignite-MSF and bitumite-MSF. The relaxation time constant (τ_0) was calculated according to the formula

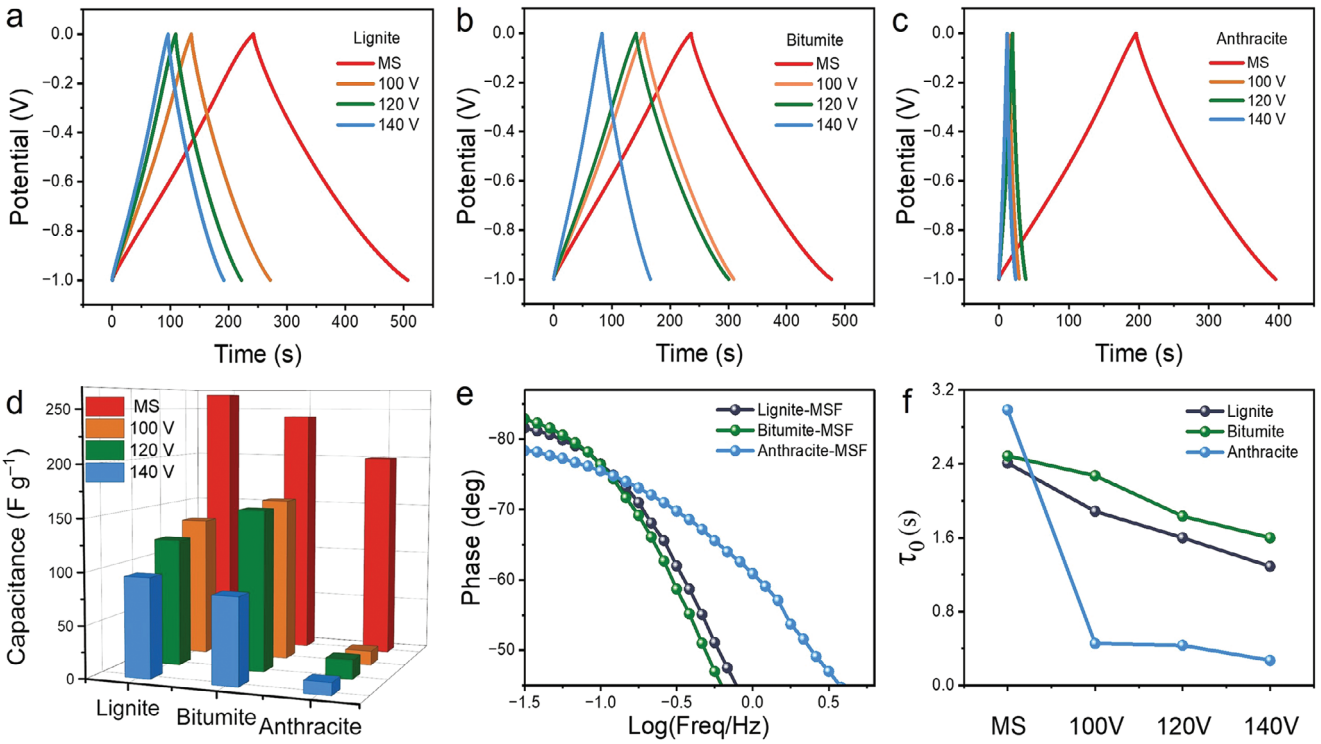

Figure 5. Galvanostatic charge-discharge (GCD) curves of a) lignite-MS and lignite-flash Joule heating (FJH) prepared at different voltages, b) bitumite-MS and bitumite-FJH prepared at different voltages, c) anthracite-MS and anthracite-FJH prepared at different voltages. d) Specific capacitance of samples in response to different applied voltages with different coals as precursors. e) The Bode plots for lignite-MSF, bitumite-MSF, and anthracite-MSF. f) Relaxation time constant of samples in response to different applied voltages with different coals as precursors.

$\tau_0 = 1/f_0$, which reflects the conductivity of the electrode.[52,53] From Figure 5f and Figure S26 (Supporting Information), we know the higher flash voltage leads to the lower τ_0 value for three coal-derived carbon materials, this is because high voltage is beneficial to the condensation of aromatic rings and the formation of large-size aromatic fragments. Notably, the electrochemical kinetics of flash carbon products could be also affected by the coal types. When the flash voltage is set as 140 V, the τ_0 values of obtained lignite-MSF, bitumite-MSF and anthracite-MSF are 1.3, 1.6, and 0.27 s, respectively. As depicted in Figure S27 (Supporting Information), the capacitive performances of the bitumite- and lignite-derived graphitized products (160 V) still conform to the rule that higher discharge voltage leads to lower capacitance and shorter relaxation time constant. The above results show that coal with low coalification tends to form carbon materials with higher capacitance, whereas anthracite is beneficial to obtain graphitic carbon materials with minimum structure defects for high rate charge storage.

3. Conclusion

In summary, the efficient FJH method enables the rapid preparation of graphitic carbons from diverse coal resources within 1 s. The resulting carbon materials exhibit obvious flake morphology, and their surface functional groups, defect concentration, and graphitization degree can be tuned during the ultrafast flash process. The structure evolution from feedstocks to products and the structure–property relationship of resultant carbons are unveiled. The anthracite tends to form long-range ordered carbon material for high rate charge storage with a higher capacity retention of 79.1% at 30 A g^{-1}, while graphitic carbon materials derived from lignite and bituminous coal with low coalification degree exhibit larger specific capacitances. This study not only sheds light on the intricate differences arising from diverse coal sources but also presents innovative avenues for enhancing the value of coal-derived materials. The comprehensive understanding gained from this research also contributes to the preparation, structure controllability, and application of coal-based carbon materials.

4. Experimental Section

Materials: Coal feedstocks including anthracite, bituminous coal, lignite, and pitch were obtained from Shanxi province, China. Potassium chloride (AR, 99.5%) and potassium carbonate (AR, 99.5%) were purchased from Aladdin Reagent Company. Sulfuric acid and potassium hydroxide were sourced from Guangzhou Chemical Reagent Factory.

FJH System: The quartz tubes (ID = 10 mm, OD = 8 mm, length = 10 cm) were used as reaction vessels. Sample powders were placed in the middle of the quartz tube, with two graphite spacers blocking both sides. Temperature changes in the FJH process were real-time monitored using a temperature detector.

Pretreatment: Firstly, the coal feedstocks were treated with ball milling for 6 h and then further grounded to 200 mesh by sand milling for an additional 6 h. Subsequently, 0.948 g KCl, 1.052 g K_2CO_3, and 0.2 g coal powders were uniformly mixed. The mixtures were heated at 750 °C for 5 h (Ar atmosphere, heating rate of 5 °C min^{-1}) in the tube furnace to fully been activated and exfoliated. Subsequently, the pretreated samples

were washed by 1.0 M sulfuric acid and distilled water to remove salts and acid-soluble impurities. The resulting materials were named as lignite-MS, bituminite-MS, and anthracite-MS, respectively.

Sample Preparation: The pretreated coal feedstocks were converted into graphitic carbon nanomaterials by ultrafast FJH process at 140 V, and the resulting products were denoted as lignite-MSF, bituminite-MSF, and anthracite-MSF. Particularly, bituminous coal was selected as the typical sample, and the effects of different flash voltages (100, 120, 140, and 160 V) on the product structure were investigated.

Characterization: The micromorphology of samples was observed by SEM (JOEL-JSM-6701) with an accelerating voltage of 7 kV. TEM images were taken from FEI-tecnai F20 with an operation voltage of 200 kV. Raman spectroscopy was performed on a Renishaw analyzer with an exciting wavelength of 532 nm. XRD measurements were conducted using Dmax2500 with Cu radiation ($2\theta^\circ$ ranging from 10° to 80°). Fourier transform infrared spectroscopy was carried out using Bruker TENSOR27. The normalization and curve-fitting of FTIR profiles were performed using Peak fit software. XPS was tested on the Thermo Scientific Nexsa. TG-IR/MS was tested using Mettler SETSYS Evolution, Bruker Tensor27, and PFEIFFER OMNI star. Element content was detected by UNICUBE-Elementar. The BET surface area and porosity were conducted by ASAP2420.

FTIR Analysis: Peaks in the range of 700–900 cm^{-1} correspond to aromatic C—H out-of-plane bending modes, while peaks at 1600 cm^{-1} correspond to C═C. Peaks in the range of 1650–1800 cm^{-1} indicate C═O groups, and peaks at 2800–3000 cm^{-1} are ascribed to aliphatic CH_X.

$$I = \frac{A_{700-900}}{A_{2800-3000}} \tag{4}$$

$$\mathrm{DOC} = \frac{A_{700-900}}{A_{1600}} \tag{5}$$

$$'C' = \frac{A_{1650-1800}}{A_{1650-1800} + A_{1600}} \tag{6}$$

Parameters: In FTIR parameter I represents the aromaticity of coal and coal rank, parameter DOC represents the condensation degree of aromatic rings, and parameter 'C' represents the maturation of coal, where *A* is the peak area of the corresponding interval.

Electrochemical Tests: For the three-electrode test, the active material, PVDF, and acetylene black were mixed in a mass ratio of 8:1:1. After stirring into a slurry, it was coated on nickel foam and used as a working electrode. Mercuric oxide electrode served as the reference electrode, a platinum plate as the counter electrode, and 6 M KOH as the electrolyte. CV, galvanostatic charge-discharge (GCD), and electrochemical impedance spectroscopy (EIS) were conducted on an electrochemical workstation (Chenhua, Shanghai, CHI660E).

Supporting Information

Supporting Information is available from the Wiley Online Library or from the author.

Acknowledgements

S.Z. and C.G. contributed equally to this work. This work was financially supported by the Fundamental Research Program of Shanxi Province (202103021223019), Science and Technology Major Project of Shanxi (No. 202101030201022).

Conflict of Interest

The authors declare no conflict of interest.

Data Availability Statement

The data that support the findings of this study are available from the corresponding author upon reasonable request.

Keywords

carbon materials, electrochemical performance, flash Joule heating, graphitization, structure

Received: March 5, 2024
Revised: July 23, 2024
Published online: August 8, 2024

[1] J. Jia, D. Wang, B. Li, *J. Mol. Struct.* **2024**, *1295*, 136655.
[2] X. Zang, Y. Dong, C. Jian, N. Ferralis, J. C. Grossman, *Matter* **2022**, *5*, 430.
[3] S. P. Sasikala, L. Henry, G. Yesilbag Tonga, K. Huang, R. Das, B. Giroire, S. Marre, V. M. Rotello, A. Penicaud, P. Poulin, C. Aymonier, *ACS Nano* **2016**, *10*, 5293.
[4] R. Deng, F. Chu, H. Yu, F. Kwofie, M. Qian, Y. Zhou, F. Wu, *Fuel Process. Technol.* **2022**, *227*, 107100.
[5] S. Hu, W. Han, X. Li, M. Ye, Y. Lu, C. Jin, Q. Liu, J. Wang, J. He, C. Cazorla, Y. Zhu, L. Chen, *Adv. Energy Mater.* **2022**, *12*, 2201469.
[6] Z. Liu, Z. Zhang, S. Choi, Y. Lu, *Energies* **2018**, *11*, 1502.
[7] S. Wang, H. Chen, X. Zhang, *Fuel* **2020**, *260*, 116309.
[8] M. Du, P. A. Advincula, X. Ding, J. M. Tour, C. Xiang, *Adv. Mater.* **2023**, *35*, 2300129.
[9] D. Dong, Y. Xiao, *Chem. Eng. J.* **2023**, *470*, 144441.
[10] Y. Chyan, R. Ye, Y. Li, S. P. Singh, C. J. Arnusch, J. M. Tour, *ACS Nano* **2018**, *12*, 2176.
[11] H. Cao, K. Li, H. Zhang, Q. Liu, *Minerals* **2023**, *13*, 749.
[12] S. Xu, J. Zhou, J. Wang, S. Pathiranage, N. Oncel, P. R. Ilango, X. Zhang, M. Mann, X. Hou, *Adv. Funct. Mater.* **2021**, *31*, 2101645.
[13] T. Cui, S. Mukherjee, P. M. Sudeep, G. Colas, F. Najafi, J. Tam, P. M. Ajayan, C. V. Singh, Y. Sun, T. Filleter, *Nat. Mater.* **2020**, *19*, 405.
[14] X. Huan, Y.-G. Tang, J.-J. Xu, C.-Y. Lan, S.-Q. Wang, *Fuel Process. Technol.* **2019**, *183*, 8.
[15] X. Zang, N. Ferralis, J. C. Grossman, *ACS Nano* **2022**, *16*, 2101.
[16] C. Li, Y. Wang, N. Xiao, H. Li, Y. Ji, Z. Guo, C. Liu, J. Qiu, *Carbon* **2019**, *151*, 46.
[17] H. Chen, N. Sun, Q. Zhu, R. A. Soomro, B. Xu, *Adv. Sci.* **2022**, *9*, 2200023.
[18] A. H. Wazir, I. u. Haq, A. Manan, A. Khan, *Int. J. Coal Prep. Util.* **2022**, *42*, 1477.
[19] Z. Zhang, J. Xiao, Q. Zhong, *Mater. Today Chem.* **2023**, *29*, 101416.
[20] W. Zhang, X. Wei, T. Wu, F. Wei, L. Ma, Y. Lv, W. Zhou, H. Liu, *Nano Energy* **2023**, *118*, 108994.
[21] F. Liu, Q. Wang, G. Zhai, H. Xiang, J. Zhou, C. Jia, L. Zhu, Q. Wu, M. Zhu, *Nat. Commun.* **2022**, *13*, 5755.
[22] X. Zang, C. Jian, S. Ingersoll, H. Li, J. J. Adams, Z. Lu, N. Ferralis, J. C. Grossman, *Sci. Adv.* **2020**, *6*, eaaz5231.
[23] T. V. Pham, J.-G. Kim, J. Y. Jung, J. H. Kim, H. Cho, T. H. Seo, H. Lee, N. D. Kim, M. J. Kim, *Adv. Funct. Mater.* **2019**, *29*, 1905511.
[24] P. Huang, R. Zhu, X. Zhang, W. Zhang, *Chem. Eng. J.* **2022**, *450*, 137999.
[25] X. Liu, H. Luo, *ACS Omega* **2024**, *9*, 2657.
[26] Y. Liao, R. Zhu, W. Zhang, Z. Liu, H. Zhu, Y. Sun, *Prog. Org. Coat.* **2023**, *184*, 107859.
[27] P. A. Advincula, W. Meng, L. J. Eddy, P. Z. Scotland, J. L. Beckham, S. Nagarajaiah, J. M. Tour, *ACS Appl. Mater. Interfaces* **2024**, *16*, 1474.

[28] P. A. Advincula, V. Granja, K. M. Wyss, W. A. Algozeeb, W. Chen, J. L. Beckham, D. X. Luong, C. F. Higgs, J. M. Tour, *Carbon* **2023**, *203*, 876.
[29] M. A. S. R. Saadi, P. A. Advincula, M. S. H. Thakur, A. Z. Khater, S. Saad, A. Shayesteh Zeraati, S. K. Nabil, A. Zinke, S. Roy, M. Lou, S. N. Bheemasetti, M. A. A. Bari, Y. Zheng, J. L. Beckham, V. Gadhamshetty, A. Vashisth, M. G. Kibria, J. M. Tour, P. M. Ajayan, M. M. Rahman, *Sci. Adv.* **2022**, *8*, eadd3555.
[30] W. Liu, J. Qi, P. Bai, W. Zhang, L. Xu, *Appl. Catal., B* **2020**, *272*, 118974.
[31] B. Tan, G. Cheng, S. Fu, H. Wang, Z. Li, X. Zhang, *Energy* **2022**, *242*, 122538.
[32] Y. Yang, J. Pan, Q. Hou, K. Wang, X. Wang, *Fuel* **2021**, *303*, 121258.
[33] J. Huang, S. Zhu, J. Zhang, G. Han, *ACS Mater. Lett.* **2024**, *6*, 2144.
[34] L. Huang, Y. Xiang, M. Luo, Q. Zhang, H. Zhu, K. Shi, S. Zhu, *Carbon* **2021**, *185*, 1.
[35] X. Zhang, G. Han, S. Zhu, *Small* **2024**, *20*, 2305406.
[36] L. Zhao, N. Guanhua, W. Hui, S. Qian, W. Gang, J. Bingyou, Z. Chao, *Fuel* **2020**, *272*, 117705.
[37] W. Yang, J. Zhou, S. Wang, Z. Wang, F. Lv, W. Zhang, W. Zhang, Q. Sun, S. Guo, *ACS Energy Lett.* **2020**, *5*, 1653.
[38] J. Jiang, W. Yang, Y. Cheng, Z. Liu, Q. Zhang, K. Zhao, *Fuel* **2019**, *239*, 559.
[39] R. Zhang, D. An, J. Zhu, X. Lu, Y. Liu, *Adv. Funct. Mater.* **2023**, *33*, 2305249.
[40] C. Ferrante, A. Virga, L. Benfatto, M. Martinati, D. De Fazio, U. Sassi, C. Fasolato, A. K. Ott, P. Postorino, D. Yoon, G. Cerullo, F. Mauri, A. C. Ferrari, T. Scopigno, *Nat. Commun.* **2018**, *9*, 308.
[41] Z. Li, L. Deng, I. A. Kinloch, R. J. Young, *Prog. Mater. Sci.* **2023**, *135*, 101089.
[42] C. Chen, Y. Tang, X. Guo, *Fuel* **2022**, *310*, 122362.
[43] K. M. Wyss, J. L. Beckham, W. Chen, D. X. Luong, P. Hundi, S. Raghuraman, R. Shahsavari, J. M. Tour, *Carbon* **2021**, *174*, 430.
[44] W. Chen, J. T. Li, Z. Wang, W. A. Algozeeb, D. X. Luong, C. Kittrell, E. A. McHugh, P. A. Advincula, K. M. Wyss, J. L. Beckham, M. G. Stanford, B. Jiang, J. M. Tour, *ACS Nano* **2021**, *15*, 11158.
[45] K. M. Wyss, D. X. Luong, J. M. Tour, *Adv. Mater.* **2022**, *34*, 2106970.
[46] W. Chen, R. V. Salvatierra, J. T. Li, C. Kittrell, J. L. Beckham, K. M. Wyss, N. La, P. E. Savas, C. Ge, P. A. Advincula, P. Scotland, L. Eddy, B. Deng, Z. Yuan, J. M. Tour, *Adv. Mater.* **2023**, *35*, 2207303.
[47] Z. Liu, C. Duan, S. Dou, Q. Yuan, J. Xu, W. D. Liu, Y. Chen, *Small* **2022**, *18*, 2200954.
[48] W. Zhang, R. Huang, X. Yan, C. Tian, Y. Xiao, Z. Lin, L. Dai, Z. Guo, L. Chai, *Angew. Chem., Int. Ed.* **2023**, *62*, 2308891.
[49] J. Wu, L. Xie, *Anal. Chem.* **2019**, *91*, 468.
[50] H. Zhang, Z. Chen, Y. Zhang, Z. Ma, Y. Zhang, L. Bai, L. Sun, *J. Mater. Chem. A* **2021**, *9*, 16565.
[51] S. F. Zhao, C. Li, Z. Cui, J. Zhang, W. Hu, R. Ma, C. M. Li, *Adv. Energy Mater.* **2023**, *13*, 2302490.
[52] N. O. Laschuk, E. B. Easton, O. V. Zenkina, *RSC Adv.* **2021**, *11*, 27925.
[53] M. DuToit, E. Ngaboyamahina, M. Wiesner, *J. Membr. Sci.* **2021**, *618*, 118680.